BABAR-CONF-04/38
SLAC-PUB-10658
August 2004

Measurement of *CP*-Violating Asymmetries in $B^0 \to (\rho\pi)^0$ Using a Time-Dependent Dalitz Plot Analysis

The *BABAR* Collaboration

February 7, 2008

Abstract

We present the preliminary measurement of *CP*-violating asymmetries in $B^0 \to (\rho\pi)^0 \to \pi^+\pi^-\pi^0$ decays using a time-dependent Dalitz plot analysis. The results are obtained from a data sample of 213 million $\Upsilon(4S) \to B\overline{B}$ decays, collected by the *BABAR* detector at the PEP-II asymmetric-energy B Factory at SLAC. This analysis extends the narrow-ρ quasi-two-body approximation used in the previous analysis, by taking into account the interference between the ρ resonances of the three charges. We measure 16 coefficients of the bilinear form factor terms occurring in the time-dependent decay rate of the B^0 meson with the use of a maximum-likelihood fit. We derive the physically relevant quantities from these coefficients. We measure the direct *CP*-violation parameters $\mathcal{A}_{\rho\pi} = -0.088 \pm 0.049 \pm 0.013$ and $C = 0.34 \pm 0.11 \pm 0.05$, where the first errors are statistical and the second systematic. For the mixing-induced *CP*-violation parameter we find $S = -0.10 \pm 0.14 \pm 0.04$, and for the dilution and strong phase shift parameters respectively, we obtain $\Delta C = 0.15 \pm 0.11 \pm 0.03$ and $\Delta S = 0.22 \pm 0.15 \pm 0.03$. For the angle α of the Unitarity Triangle we measure $(113\,^{+27}_{-17} \pm 6)^\circ$, while only a weak constraint is achieved at the significance level of more than two standard deviations. Finally, for the relative strong phase δ_{+-} between the $B^0 \to \rho^-\pi^+$ and $B^0 \to \rho^+\pi^-$ transitions we find $(-67\,^{+28}_{-31} \pm 7)^\circ$, with a similarly weak constraint at two standard deviations and beyond.

Submitted to the 32nd International Conference on High-Energy Physics, ICHEP 04,
16 August—22 August 2004, Beijing, China

Stanford Linear Accelerator Center, Stanford University, Stanford, CA 94309

Work supported in part by Department of Energy contract DE-AC03-76SF00515.

The *BABAR* Collaboration,

B. Aubert, R. Barate, D. Boutigny, F. Couderc, J.-M. Gaillard, A. Hicheur, Y. Karyotakis, J. P. Lees, V. Tisserand, A. Zghiche

Laboratoire de Physique des Particules, F-74941 Annecy-le-Vieux, France

A. Palano, A. Pompili

Università di Bari, Dipartimento di Fisica and INFN, I-70126 Bari, Italy

J. C. Chen, N. D. Qi, G. Rong, P. Wang, Y. S. Zhu

Institute of High Energy Physics, Beijing 100039, China

G. Eigen, I. Ofte, B. Stugu

University of Bergen, Inst. of Physics, N-5007 Bergen, Norway

G. S. Abrams, A. W. Borgland, A. B. Breon, D. N. Brown, J. Button-Shafer, R. N. Cahn, E. Charles, C. T. Day, M. S. Gill, A. V. Gritsan, Y. Groysman, R. G. Jacobsen, R. W. Kadel, J. Kadyk, L. T. Kerth, Yu. G. Kolomensky, G. Kukartsev, G. Lynch, L. M. Mir, P. J. Oddone, T. J. Orimoto, M. Pripstein, N. A. Roe, M. T. Ronan, V. G. Shelkov, W. A. Wenzel

Lawrence Berkeley National Laboratory and University of California, Berkeley, CA 94720, USA

M. Barrett, K. E. Ford, T. J. Harrison, A. J. Hart, C. M. Hawkes, S. E. Morgan, A. T. Watson

University of Birmingham, Birmingham, B15 2TT, United Kingdom

M. Fritsch, K. Goetzen, T. Held, H. Koch, B. Lewandowski, M. Pelizaeus, M. Steinke

Ruhr Universität Bochum, Institut für Experimentalphysik 1, D-44780 Bochum, Germany

J. T. Boyd, N. Chevalier, W. N. Cottingham, M. P. Kelly, T. E. Latham, F. F. Wilson

University of Bristol, Bristol BS8 1TL, United Kingdom

T. Cuhadar-Donszelmann, C. Hearty, N. S. Knecht, T. S. Mattison, J. A. McKenna, D. Thiessen

University of British Columbia, Vancouver, BC, Canada V6T 1Z1

A. Khan, P. Kyberd, L. Teodorescu

Brunel University, Uxbridge, Middlesex UB8 3PH, United Kingdom

A. E. Blinov, V. E. Blinov, V. P. Druzhinin, V. B. Golubev, V. N. Ivanchenko, E. A. Kravchenko, A. P. Onuchin, S. I. Serednyakov, Yu. I. Skovpen, E. P. Solodov, A. N. Yushkov

Budker Institute of Nuclear Physics, Novosibirsk 630090, Russia

D. Best, M. Bruinsma, M. Chao, I. Eschrich, D. Kirkby, A. J. Lankford, M. Mandelkern, R. K. Mommsen, W. Roethel, D. P. Stoker

University of California at Irvine, Irvine, CA 92697, USA

C. Buchanan, B. L. Hartfiel

University of California at Los Angeles, Los Angeles, CA 90024, USA

S. D. Foulkes, J. W. Gary, B. C. Shen, K. Wang

University of California at Riverside, Riverside, CA 92521, USA

D. del Re, H. K. Hadavand, E. J. Hill, D. B. MacFarlane, H. P. Paar, Sh. Rahatlou, V. Sharma

University of California at San Diego, La Jolla, CA 92093, USA

J. W. Berryhill, C. Campagnari, B. Dahmes, O. Long, A. Lu, M. A. Mazur, J. D. Richman, W. Verkerke

University of California at Santa Barbara, Santa Barbara, CA 93106, USA

T. W. Beck, A. M. Eisner, C. A. Heusch, J. Kroseberg, W. S. Lockman, G. Nesom, T. Schalk, B. A. Schumm, A. Seiden, P. Spradlin, D. C. Williams, M. G. Wilson

University of California at Santa Cruz, Institute for Particle Physics, Santa Cruz, CA 95064, USA

J. Albert, E. Chen, G. P. Dubois-Felsmann, A. Dvoretskii, D. G. Hitlin, I. Narsky, T. Piatenko, F. C. Porter, A. Ryd, A. Samuel, S. Yang

California Institute of Technology, Pasadena, CA 91125, USA

S. Jayatilleke, G. Mancinelli, B. T. Meadows, M. D. Sokoloff

University of Cincinnati, Cincinnati, OH 45221, USA

T. Abe, F. Blanc, P. Bloom, S. Chen, W. T. Ford, U. Nauenberg, A. Olivas, P. Rankin, J. G. Smith, J. Zhang, L. Zhang

University of Colorado, Boulder, CO 80309, USA

A. Chen, J. L. Harton, A. Soffer, W. H. Toki, R. J. Wilson, Q. Zeng

Colorado State University, Fort Collins, CO 80523, USA

D. Altenburg, T. Brandt, J. Brose, M. Dickopp, E. Feltresi, A. Hauke, H. M. Lacker, R. Müller-Pfefferkorn, R. Nogowski, S. Otto, A. Petzold, J. Schubert, K. R. Schubert, R. Schwierz, B. Spaan, J. E. Sundermann

Technische Universität Dresden, Institut für Kern- und Teilchenphysik, D-01062 Dresden, Germany

D. Bernard, G. R. Bonneaud, F. Brochard, P. Grenier, S. Schrenk, Ch. Thiebaux, G. Vasileiadis, M. Verderi

Ecole Polytechnique, LLR, F-91128 Palaiseau, France

D. J. Bard, P. J. Clark, D. Lavin, F. Muheim, S. Playfer, Y. Xie

University of Edinburgh, Edinburgh EH9 3JZ, United Kingdom

M. Andreotti, V. Azzolini, D. Bettoni, C. Bozzi, R. Calabrese, G. Cibinetto, E. Luppi, M. Negrini, L. Piemontese, A. Sarti

Università di Ferrara, Dipartimento di Fisica and INFN, I-44100 Ferrara, Italy

E. Treadwell

Florida A&M University, Tallahassee, FL 32307, USA

F. Anulli, R. Baldini-Ferroli, A. Calcaterra, R. de Sangro, G. Finocchiaro, P. Patteri, I. M. Peruzzi, M. Piccolo, A. Zallo

Laboratori Nazionali di Frascati dell'INFN, I-00044 Frascati, Italy

A. Buzzo, R. Capra, R. Contri, G. Crosetti, M. Lo Vetere, M. Macri, M. R. Monge, S. Passaggio, C. Patrignani, E. Robutti, A. Santroni, S. Tosi

Università di Genova, Dipartimento di Fisica and INFN, I-16146 Genova, Italy

S. Bailey, G. Brandenburg, K. S. Chaisanguanthum, M. Morii, E. Won

Harvard University, Cambridge, MA 02138, USA

R. S. Dubitzky, U. Langenegger

Universität Heidelberg, Physikalisches Institut, Philosophenweg 12, D-69120 Heidelberg, Germany

W. Bhimji, D. A. Bowerman, P. D. Dauncey, U. Egede, J. R. Gaillard, G. W. Morton, J. A. Nash, M. B. Nikolich, G. P. Taylor

Imperial College London, London, SW7 2AZ, United Kingdom

M. J. Charles, G. J. Grenier, U. Mallik

University of Iowa, Iowa City, IA 52242, USA

J. Cochran, H. B. Crawley, J. Lamsa, W. T. Meyer, S. Prell, E. I. Rosenberg, A. E. Rubin, J. Yi

Iowa State University, Ames, IA 50011-3160, USA

M. Biasini, R. Covarelli, M. Pioppi

Università di Perugia, Dipartimento di Fisica and INFN, I-06100 Perugia, Italy

M. Davier, X. Giroux, G. Grosdidier, A. Höcker, S. Laplace, F. Le Diberder, V. Lepeltier, A. M. Lutz, T. C. Petersen, S. Plaszczynski, M. H. Schune, L. Tantot, G. Wormser

Laboratoire de l'Accélérateur Linéaire, F-91898 Orsay, France

C. H. Cheng, D. J. Lange, M. C. Simani, D. M. Wright

Lawrence Livermore National Laboratory, Livermore, CA 94550, USA

A. J. Bevan, C. A. Chavez, J. P. Coleman, I. J. Forster, J. R. Fry, E. Gabathuler, R. Gamet, D. E. Hutchcroft, R. J. Parry, D. J. Payne, R. J. Sloane, C. Touramanis

University of Liverpool, Liverpool L69 72E, United Kingdom

J. J. Back,[1] C. M. Cormack, P. F. Harrison,[1] F. Di Lodovico, G. B. Mohanty[1]

Queen Mary, University of London, E1 4NS, United Kingdom

C. L. Brown, G. Cowan, R. L. Flack, H. U. Flaecher, M. G. Green, P. S. Jackson, T. R. McMahon, S. Ricciardi, F. Salvatore, M. A. Winter

University of London, Royal Holloway and Bedford New College, Egham, Surrey TW20 0EX, United Kingdom

D. Brown, C. L. Davis

University of Louisville, Louisville, KY 40292, USA

J. Allison, N. R. Barlow, R. J. Barlow, P. A. Hart, M. C. Hodgkinson, G. D. Lafferty, A. J. Lyon, J. C. Williams

University of Manchester, Manchester M13 9PL, United Kingdom

A. Farbin, W. D. Hulsbergen, A. Jawahery, D. Kovalskyi, C. K. Lae, V. Lillard, D. A. Roberts

University of Maryland, College Park, MD 20742, USA

G. Blaylock, C. Dallapiccola, K. T. Flood, S. S. Hertzbach, R. Kofler, V. B. Koptchev, T. B. Moore, S. Saremi, H. Staengle, S. Willocq

University of Massachusetts, Amherst, MA 01003, USA

[1]Now at Department of Physics, University of Warwick, Coventry, United Kingdom

R. Cowan, G. Sciolla, S. J. Sekula, F. Taylor, R. K. Yamamoto

Massachusetts Institute of Technology, Laboratory for Nuclear Science, Cambridge, MA 02139, USA

D. J. J. Mangeol, P. M. Patel, S. H. Robertson

McGill University, Montréal, QC, Canada H3A 2T8

A. Lazzaro, V. Lombardo, F. Palombo

Università di Milano, Dipartimento di Fisica and INFN, I-20133 Milano, Italy

J. M. Bauer, L. Cremaldi, V. Eschenburg, R. Godang, R. Kroeger, J. Reidy, D. A. Sanders, D. J. Summers, H. W. Zhao

University of Mississippi, University, MS 38677, USA

S. Brunet, D. Côté, P. Taras

Université de Montréal, Laboratoire René J. A. Lévesque, Montréal, QC, Canada H3C 3J7

H. Nicholson

Mount Holyoke College, South Hadley, MA 01075, USA

N. Cavallo,[2] F. Fabozzi,[2] C. Gatto, L. Lista, D. Monorchio, P. Paolucci, D. Piccolo, C. Sciacca

Università di Napoli Federico II, Dipartimento di Scienze Fisiche and INFN, I-80126, Napoli, Italy

M. Baak, H. Bulten, G. Raven, H. L. Snoek, L. Wilden

NIKHEF, National Institute for Nuclear Physics and High Energy Physics, NL-1009 DB Amsterdam, The Netherlands

C. P. Jessop, J. M. LoSecco

University of Notre Dame, Notre Dame, IN 46556, USA

T. Allmendinger, K. K. Gan, K. Honscheid, D. Hufnagel, H. Kagan, R. Kass, T. Pulliam, A. M. Rahimi, R. Ter-Antonyan, Q. K. Wong

Ohio State University, Columbus, OH 43210, USA

J. Brau, R. Frey, O. Igonkina, C. T. Potter, N. B. Sinev, D. Strom, E. Torrence

University of Oregon, Eugene, OR 97403, USA

F. Colecchia, A. Dorigo, F. Galeazzi, M. Margoni, M. Morandin, M. Posocco, M. Rotondo, F. Simonetto, R. Stroili, G. Tiozzo, C. Voci

Università di Padova, Dipartimento di Fisica and INFN, I-35131 Padova, Italy

M. Benayoun, H. Briand, J. Chauveau, P. David, Ch. de la Vaissière, L. Del Buono, O. Hamon, M. J. J. John, Ph. Leruste, J. Malcles, J. Ocariz, M. Pivk, L. Roos, S. T'Jampens, G. Therin

Universités Paris VI et VII, Laboratoire de Physique Nucléaire et de Hautes Energies, F-75252 Paris, France

P. F. Manfredi, V. Re

Università di Pavia, Dipartimento di Elettronica and INFN, I-27100 Pavia, Italy

[2]Also with Università della Basilicata, Potenza, Italy

P. K. Behera, L. Gladney, Q. H. Guo, J. Panetta

University of Pennsylvania, Philadelphia, PA 19104, USA

C. Angelini, G. Batignani, S. Bettarini, M. Bondioli, F. Bucci, G. Calderini, M. Carpinelli, F. Forti, M. A. Giorgi, A. Lusiani, G. Marchiori, F. Martinez-Vidal,[3] M. Morganti, N. Neri, E. Paoloni, M. Rama, G. Rizzo, F. Sandrelli, J. Walsh

Università di Pisa, Dipartimento di Fisica, Scuola Normale Superiore and INFN, I-56127 Pisa, Italy

M. Haire, D. Judd, K. Paick, D. E. Wagoner

Prairie View A&M University, Prairie View, TX 77446, USA

N. Danielson, P. Elmer, Y. P. Lau, C. Lu, V. Miftakov, J. Olsen, A. J. S. Smith, A. V. Telnov

Princeton University, Princeton, NJ 08544, USA

F. Bellini, G. Cavoto,[4] R. Faccini, F. Ferrarotto, F. Ferroni, M. Gaspero, L. Li Gioi, M. A. Mazzoni, S. Morganti, M. Pierini, G. Piredda, F. Safai Tehrani, C. Voena

Università di Roma La Sapienza, Dipartimento di Fisica and INFN, I-00185 Roma, Italy

S. Christ, G. Wagner, R. Waldi

Universität Rostock, D-18051 Rostock, Germany

T. Adye, N. De Groot, B. Franek, N. I. Geddes, G. P. Gopal, E. O. Olaiya

Rutherford Appleton Laboratory, Chilton, Didcot, Oxon, OX11 0QX, United Kingdom

R. Aleksan, S. Emery, A. Gaidot, S. F. Ganzhur, P.-F. Giraud, G. Hamel de Monchenault, W. Kozanecki, M. Legendre, G. W. London, B. Mayer, G. Schott, G. Vasseur, Ch. Yèche, M. Zito

DSM/Dapnia, CEA/Saclay, F-91191 Gif-sur-Yvette, France

M. V. Purohit, A. W. Weidemann, J. R. Wilson, F. X. Yumiceva

University of South Carolina, Columbia, SC 29208, USA

D. Aston, R. Bartoldus, N. Berger, A. M. Boyarski, O. L. Buchmueller, R. Claus, M. R. Convery, M. Cristinziani, G. De Nardo, D. Dong, J. Dorfan, D. Dujmic, W. Dunwoodie, E. E. Elsen, S. Fan, R. C. Field, T. Glanzman, S. J. Gowdy, T. Hadig, V. Halyo, C. Hast, T. Hryn'ova, W. R. Innes, M. H. Kelsey, P. Kim, M. L. Kocian, D. W. G. S. Leith, J. Libby, S. Luitz, V. Luth, H. L. Lynch, H. Marsiske, R. Messner, D. R. Muller, C. P. O'Grady, V. E. Ozcan, A. Perazzo, M. Perl, S. Petrak, B. N. Ratcliff, A. Roodman, A. A. Salnikov, R. H. Schindler, J. Schwiening, G. Simi, A. Snyder, A. Soha, J. Stelzer, D. Su, M. K. Sullivan, J. Va'vra, S. R. Wagner, M. Weaver, A. J. R. Weinstein, W. J. Wisniewski, M. Wittgen, D. H. Wright, A. K. Yarritu, C. C. Young

Stanford Linear Accelerator Center, Stanford, CA 94309, USA

P. R. Burchat, A. J. Edwards, T. I. Meyer, B. A. Petersen, C. Roat

Stanford University, Stanford, CA 94305-4060, USA

S. Ahmed, M. S. Alam, J. A. Ernst, M. A. Saeed, M. Saleem, F. R. Wappler

State University of New York, Albany, NY 12222, USA

[3]Also with IFIC, Instituto de Física Corpuscular, CSIC-Universidad de Valencia, Valencia, Spain
[4]Also with Princeton University, Princeton, USA

W. Bugg, M. Krishnamurthy, S. M. Spanier
University of Tennessee, Knoxville, TN 37996, USA

R. Eckmann, H. Kim, J. L. Ritchie, A. Satpathy, R. F. Schwitters
University of Texas at Austin, Austin, TX 78712, USA

J. M. Izen, I. Kitayama, X. C. Lou, S. Ye
University of Texas at Dallas, Richardson, TX 75083, USA

F. Bianchi, M. Bona, F. Gallo, D. Gamba
Università di Torino, Dipartimento di Fisica Sperimentale and INFN, I-10125 Torino, Italy

L. Bosisio, C. Cartaro, F. Cossutti, G. Della Ricca, S. Dittongo, S. Grancagnolo, L. Lanceri, P. Poropat,[5] L. Vitale, G. Vuagnin
Università di Trieste, Dipartimento di Fisica and INFN, I-34127 Trieste, Italy

R. S. Panvini
Vanderbilt University, Nashville, TN 37235, USA

Sw. Banerjee, C. M. Brown, D. Fortin, P. D. Jackson, R. Kowalewski, J. M. Roney, R. J. Sobie
University of Victoria, Victoria, BC, Canada V8W 3P6

H. R. Band, B. Cheng, S. Dasu, M. Datta, A. M. Eichenbaum, M. Graham, J. J. Hollar, J. R. Johnson, P. E. Kutter, H. Li, R. Liu, A. Mihalyi, A. K. Mohapatra, Y. Pan, R. Prepost, P. Tan, J. H. von Wimmersperg-Toeller, J. Wu, S. L. Wu, Z. Yu
University of Wisconsin, Madison, WI 53706, USA

M. G. Greene, H. Neal
Yale University, New Haven, CT 06511, USA

[5]Deceased

1 INTRODUCTION

Measurements of the parameter sin2β [1,2] have established *CP* violation in the B^0 meson system and provide strong support for the Kobayashi and Maskawa model of this phenomenon as arising from a single phase in the three-generation CKM quark-mixing matrix [3]. We present in this letter preliminary results from a time-dependent analysis of the $B^0 \to \pi^+\pi^-\pi^0$ Dalitz plot (DP) that is dominated by the ρ intermediate resonances. The goal of the analysis is the simultaneous extraction of the strong transition amplitudes and the weak interaction phase $\alpha \equiv \arg\left[-V_{td}V_{tb}^*/V_{ud}V_{ub}^*\right]$ of the Unitarity Triangle. In the Standard Model, a non-zero value for α would be responsible for the occurrence of mixing-induced *CP* violation in this decay. The *BABAR* and Belle experiments have obtained constraints on α from the measurement of effective quantities sin2$\alpha_{\rm eff}$ in B decays to $\pi^+\pi^-$ [4,5] and *BABAR* from B decays to $\rho^+\rho^-$ [6], using an isospin analysis [7] that involves the other charges of these final states to obtain bounds on $\alpha - \alpha_{\rm eff}$.

Unlike $\pi^+\pi^-$, $\rho^\pm\pi^\mp$ is not a *CP* eigenstate, and four flavor-charge configurations ($B^0(\overline{B}^0) \to \rho^\pm\pi^\mp$) must be considered. The corresponding isospin analysis [8] is unfruitful with the present statistics since two pentagonal amplitude relations with 12 unknowns have to be solved (compared to 6 unknowns for the $\pi^+\pi^-$ and $\rho^+\rho^-$ systems). However, it has been pointed out by Snyder and Quinn [9], that one can obtain the necessary degrees of freedom to constrain α without ambiguity by explicitly including in the analysis the variation of the strong phases of the interfering ρ resonances in the Dalitz plot.

The present analysis focuses on the decay $B^0 \to (\rho\pi)^0 \to \pi^+\pi^-\pi^0$. The data sample used is a superset of that used for our previous time-dependent result [10], obtained within the quasi-two-body approximation. In that approach, the analysis was restricted to the charged-ρ regions in the Dalitz plot, and the interference regions were removed. Here, we extend the analysis to the entire region of interest in the Dalitz plot, which contains the ρ resonances of all three charges and their interference.

1.1 DECAY AMPLITUDES

We consider the decay of a spin-zero B^0 with four-momentum p_B into the three daughters $\pi^+(p_+)$, $\pi^-(p_-)$, $\pi^0(p_0)$, with corresponding four-momenta. Using as independent (Mandelstam) variables the invariant masses-squared

$$s_+ \;=\; (p_+ + p_0)^2 \;, \qquad s_- \;=\; (p_- + p_0)^2 \;, \tag{1}$$

the invariant mass of the positive and negative pion, $s_0 \;=\; (p_+ + p_-)^2$, is obtained from energy and momentum conservation

$$s_0 \;=\; m_{B^0}^2 + 2m_{\pi^+}^2 + m_{\pi^0}^2 - s_+ - s_- \;. \tag{2}$$

The differential B^0 decay width with respect to the variables defined in Eq. (1) (*i.e.*, the *Dalitz plot*) reads

$$d\Gamma(B^0 \to \pi^+\pi^-\pi^0) \;=\; \frac{1}{(2\pi)^3}\frac{|\mathcal{A}_{3\pi}|^2}{8m_{B^0}^3}\,ds_+ ds_- \;, \tag{3}$$

where $\mathcal{A}_{3\pi}$ is the Lorentz-invariant amplitude of the three-body decay.

We assume in the following that the amplitudes $\mathcal{A}_{3\pi}$ and its complex conjugate $\overline{\mathcal{A}}_{3\pi}$, corresponding to the transitions $B^0 \to \pi^+\pi^-\pi^0$ and $\overline{B}^0 \to \pi^+\pi^-\pi^0$, respectively, are dominated by the

three resonances ρ^+, ρ^- and ρ^0. The ρ resonances are assumed to be the sum of the ground state $\rho(770)$ and the radial excitations $\rho(1450)$ and $\rho(1700)$, with an initial set of resonance parameters and relative amplitudes determined by a combined fit to $\tau^+ \to \overline{\nu}_\tau \pi^+ \pi^0$ and $e^+e^- \to \pi^+\pi^-$ data [11]. Since the hadronic environment is different in B decays, we cannot rely on this result and therefore determine the relative $\rho(1450)$ amplitude simultaneously with the *CP* parameters from the fit. Variations of the other parameters and possible contributions to the $B^0 \to \pi^+\pi^-\pi^0$ decay other than the ρ's are studied as part of the systematic uncertainties (Section 4).

Including the $B^0\overline{B}^0$ mixing parameter q/p into the $\overline{B}^0$ decay amplitudes, we can write [9,12]

$$\mathcal{A}_{3\pi} = f_+ A^+ + f_- A^- + f_0 A^0 \,, \tag{4}$$

$$\overline{\mathcal{A}}_{3\pi} = f_+ \overline{A}^+ + f_- \overline{A}^- + f_0 \overline{A}^0 \,, \tag{5}$$

where the f_κ (with the ρ charge $\kappa = \{+,-,0\}$) are functions of the Dalitz variables s_+ and s_- that incorporate the kinematic and dynamical properties of the B^0 decay into a (vector) ρ resonance and a (pseudoscalar) pion, and where the A^κ are complex amplitudes[6] that may comprise weak and strong transition phases and that are independent of the Dalitz variables. Note that the definitions (4) and (5) imply the assumption that the relative phases between the $\rho(770)$ and its radial excitations are *CP*-conserving.

Following Ref. [11], the ρ resonances are parameterized by a modified relativistic Breit-Wigner function introduced by Gounaris and Sakurai (GS) [15]. Due to angular momentum conservation, the spin-one ρ resonance is polarized in a helicity-zero state. For a ρ^κ resonance with charge κ, the GS function is multiplied by the kinematic function $-4|\mathbf{p}_\kappa||\mathbf{p}_\tau|\cos\theta_\kappa$, where the momenta are defined in the ρ-resonance rest frame, and where $\mathbf{p}_\tau$ is the momentum of the particle not from ρ decay, and $\cos\theta_\kappa$ the cosine of the helicity angle of the ρ^κ. For the ρ^+ (ρ^-), θ_+ (θ_-) is defined by the angle between the π^0 (π^-) in the ρ^+ (ρ^-) rest frame and the ρ^+ (ρ^-) flight direction in the B^0 rest frame. For the ρ^0, θ_0 is defined by the angle between the π^+ in the ρ^0 rest frame and the ρ^0 flight direction in the B^0 rest frame. With these definitions, each pair of GS functions interferes destructively at equal masses-squared.

The occurrence of $\cos\theta_\kappa$ in the kinematic functions substantially enhances the interference between the different ρ bands in the Dalitz plot, and thus increases the sensitivity of this analysis [9].

1.2 TIME DEPENDENCE

With $\Delta t \equiv t_{3\pi} - t_{\rm tag}$ defined as the proper time interval between the decay of the fully reconstructed $B^0_{3\pi}$ and that of the other meson $B^0_{\rm tag}$, the time-dependent decay rate $|\mathcal{A}^+_{3\pi}(\Delta t)|^2$ ($|\mathcal{A}^-_{3\pi}(\Delta t)|^2$) when the tagging meson is a B^0 ($\overline{B}^0$) is given by

$$|\mathcal{A}^\pm_{3\pi}(\Delta t)|^2 = \frac{e^{-|\Delta t|/\tau_{B^0}}}{4\tau_{B^0}} \Big[|\mathcal{A}_{3\pi}|^2 + |\overline{\mathcal{A}}_{3\pi}|^2 \mp \left(|\mathcal{A}_{3\pi}|^2 - |\overline{\mathcal{A}}_{3\pi}|^2 \right) \cos(\Delta m_d \Delta t) \pm 2{\rm Im}\left[\overline{\mathcal{A}}_{3\pi} \mathcal{A}^*_{3\pi} \right] \sin(\Delta m_d \Delta t) \Big] \,, \tag{6}$$

where τ_{B^0} is the mean B^0 lifetime, Δm_d is the $B^0\overline{B}^0$ oscillation frequency, and where we have assumed that *CP* violation in $B^0\overline{B}^0$ mixing is absent ($|q/p| = 1$), $\Delta\Gamma_{B_d} = 0$ and *CPT* is conserved.

[6] The amplitude superscript "κ" denotes the charge of the ρ from the decay of the B^0 meson.

Inserting the amplitudes (4) and (5), one obtains for the terms in Eq. (6)

$$
\begin{aligned}
|\mathcal{A}_{3\pi}|^2 \pm |\overline{\mathcal{A}}_{3\pi}|^2 &= \sum_{\kappa\in\{+,-,0\}} |f_\kappa|^2 U_\kappa^\pm + 2\sum_{\kappa<\sigma\in\{+,-,0\}} \Big(\mathrm{Re}\left[f_\kappa f_\sigma^*\right] U_{\kappa\sigma}^{\pm,\mathrm{Re}} - \mathrm{Im}\left[f_\kappa f_\sigma^*\right] U_{\kappa\sigma}^{\pm,\mathrm{Im}} \Big) \ , \\
\mathrm{Im}\left(\overline{\mathcal{A}}_{3\pi}\mathcal{A}_{3\pi}^\star\right) &= \sum_{\kappa\in\{+,-,0\}} |f_\kappa|^2 I_\kappa + \sum_{\kappa<\sigma\in\{+,-,0\}} \Big(\mathrm{Re}\left[f_\kappa f_\sigma^*\right] I_{\kappa\sigma}^{\mathrm{Im}} + \mathrm{Im}\left[f_\kappa f_\sigma^*\right] I_{\kappa\sigma}^{\mathrm{Re}} \Big) \ ,
\end{aligned} \tag{7}
$$

with

$$
\begin{aligned}
U_\kappa^\pm &= |A^\kappa|^2 \pm |\overline{A}^\kappa|^2 \ , & (8)\\
U_{\kappa\sigma}^{\pm,\mathrm{Re(Im)}} &= \mathrm{Re(Im)}\left[A^\kappa A^{\sigma *} \pm \overline{A}^\kappa \overline{A}^{\sigma *}\right] \ , & (9)\\
I_\kappa &= \mathrm{Im}\left[\overline{A}^\kappa A^{\kappa *}\right] \ , & (10)\\
I_{\kappa\sigma}^{\mathrm{Re}} &= \mathrm{Re}\left[\overline{A}^\kappa A^{\sigma *} - \overline{A}^\sigma A^{\kappa *}\right] \ , & (11)\\
I_{\kappa\sigma}^{\mathrm{Im}} &= \mathrm{Im}\left[\overline{A}^\kappa A^{\sigma *} + \overline{A}^\sigma A^{\kappa *}\right] \ . & (12)
\end{aligned}
$$

The 27 coefficients (8)–(12) are real-valued parameters that multiply the $f_\kappa f_\sigma^*$ bilinears [16]. They are the observables that are determined by the fit. Each of the coefficients is related in a unique way to the physically more intuitive quantities, like tree-level and penguin-type amplitudes, the angle α, or the quasi-two-body *CP* and dilution parameters [10] (*cf.* Section 6).

The U_κ^+ coefficients are related to resonance fractions (branching fractions and charge asymmetries), the U_κ^- determine the relative abundance of the B^0 decay into $\rho^+\pi^-$ and $\rho^-\pi^+$ (dilution) and the time-dependent direct *CP* asymmetries. The I_κ measure mixing-induced *CP* violation and are sensitive to strong phase shifts. Finally, the $U_{\kappa\sigma}^{\pm,\mathrm{Re(Im)}}$ and $I_{\kappa\sigma}^{\mathrm{Re(Im)}}$ describe the interference pattern in the Dalitz plot. Their presence distinguishes this analysis from the previous quasi-two-body one [10]. They represent the additional degrees of freedom that allows one to determine the unknown penguin pollution and the relative strong phases. However, because the overlap regions of the resonances are small and because the event reconstruction in these regions suffers from large misreconstruction rates and background, a substantial data sample is needed to perform a fit that constrains all amplitude parameters.

The choice to fit for the U and I coefficients rather than fitting for the complex transition amplitudes and the weak phase α directly is motivated by the following technical simplifications: (*i*) in contrast to the amplitudes, there is a unique solution for the U and I coefficients requiring only a single fit to the selected data sample[7], (*ii*) in the presence of background, the U and I coefficients are approximately Gaussian distributed, which in general is not the case for the amplitudes, and (*iii*) the propagation of systematic uncertainties and the averaging between different measurements are straightforward for the U's and I's.

We determine the quantities of interest in a subsequent least-squares fit to the measured U and I coefficients.

[7]The parameterization (7) is general: the information on the mirror solutions (*e.g.*, on the angle α) that are present in the transition amplitudes A^κ, $\overline{A}^\kappa$ is conserved.

1.3 NORMALIZATION

The decay rate (6) is used as probability density function (PDF) in a maximum-likelihood fit and must therefore be normalized:

$$|\mathcal{A}_{3\pi}^{\pm}(\Delta t)|^2 \;\longrightarrow\; \frac{1}{\langle |\mathcal{A}_{3\pi}|^2 + |\overline{\mathcal{A}}_{3\pi}|^2 \rangle} |\mathcal{A}_{3\pi}^{\pm}(\Delta t)|^2 \;, \tag{13}$$

where

$$\langle |\mathcal{A}_{3\pi}|^2 + |\overline{\mathcal{A}}_{3\pi}|^2 \rangle \;=\; \sum_{\kappa \in \{+,-,0\}} \langle |f_\kappa|^2 \rangle U_\kappa^+ \;+\; 2\mathrm{Re} \sum_{\kappa < \sigma \in \{+,-,0\}} \langle f_\kappa f_\sigma^* \rangle \left(U_{\kappa\sigma}^{+,\mathrm{Re}} + i \cdot U_{\kappa\sigma}^{+,\mathrm{Im}} \right) \;. \tag{14}$$

The complex expectation values $\langle f_\kappa f_\sigma^* \rangle$ are obtained from high-statistics Monte Carlo integration of the Dalitz plot (3), taking into account acceptance and resolution effects.

The normalization of the decay rate (6) renders the normalization of the U and I coefficients arbitrary, so that we can fix one coefficient. By convention, we set $U_+^+ \equiv 1$.

For a small $B^0 \to \rho^0\pi^0$ signal, the time-dependent *CP* information from this mode is marginal. As a consequence, we are allowed to simplify the model by setting the coefficients of the sine and cosine terms that involve this mode to zero, which entails only a small systematic error on the result. This reduces the number of free parameters from 26 to 16.

1.4 THE SQUARE DALITZ PLOT

The signal events and also the combinatorial $e^+e^- \to q\bar{q}$ ($q = u, d, s, c$) continuum background events populate the kinematic boundaries of the Dalitz plot due to the low final state masses compared to the B^0 mass. Hence the representation Eq. (3) is inadequate when one wants to use empirical reference shapes in a maximum-likelihood fit. Another practical disadvantage of the Dalitz variables is that they are not constant along the kinematic boundaries of the $B^0 \to \pi^+\pi^-\pi^0$ Dalitz plot, which complicates the correction of efficiency and resolution effects. We therefore apply the transformation

$$ds_+ \, ds_- \;\longrightarrow |\det J| \, dm' \, d\theta' \;, \tag{15}$$

which defines the *Square Dalitz plot* (SDP). The new coordinates are

$$m' \;\equiv\; \frac{1}{\pi} \arccos\left(2 \frac{m_0 - m_0^{\min}}{m_0^{\max} - m_0^{\min}} - 1 \right) \;, \quad \text{and} \quad \theta' \;\equiv\; \frac{1}{\pi}\theta_0 \;, \tag{16}$$

where m_0 is the invariant mass between the charged tracks, $m_0^{\max} = m_{B^0} - m_{\pi^0}$ and $m_0^{\min} = 2m_{\pi^+}$ are the kinematic limits of m_0, θ_0 is the ρ^0 helicity angle, and J is the Jacobian of the transformation that zooms into the kinematic boundaries of the Dalitz plot. The new variables have validity ranges between 0 and 1. The determinant of the Jacobian is given by

$$|\det J| \;=\; 4\,|\mathbf{p}_+^*||\mathbf{p}_0^*|\, m_0 \cdot \frac{\partial m_0}{\partial m'} \cdot \frac{\partial \cos\theta_0}{\partial \theta'} \;, \tag{17}$$

where $|\mathbf{p}_+^*| = \sqrt{E_+^{*} - m_{\pi^+}^2}$ and $|\mathbf{p}_0^*| = \sqrt{E_0^{*} - m_{\pi^0}^2}$, and where the energies E_+^* and E_0^* are in the $\pi^+\pi^-$ rest frame.

Figure 1 shows the original (left hand plot) and the transformed (right hand plot) Dalitz plots for Monte Carlo $B^0 \to \pi^+\pi^-\pi^0$ events generated according to Eqs. (4) and (5) with equal abundance of all ρ charges and with vanishing relative strong phase. The plots illustrate the homogenization of the Dalitz plot obtained after the transformation (15).

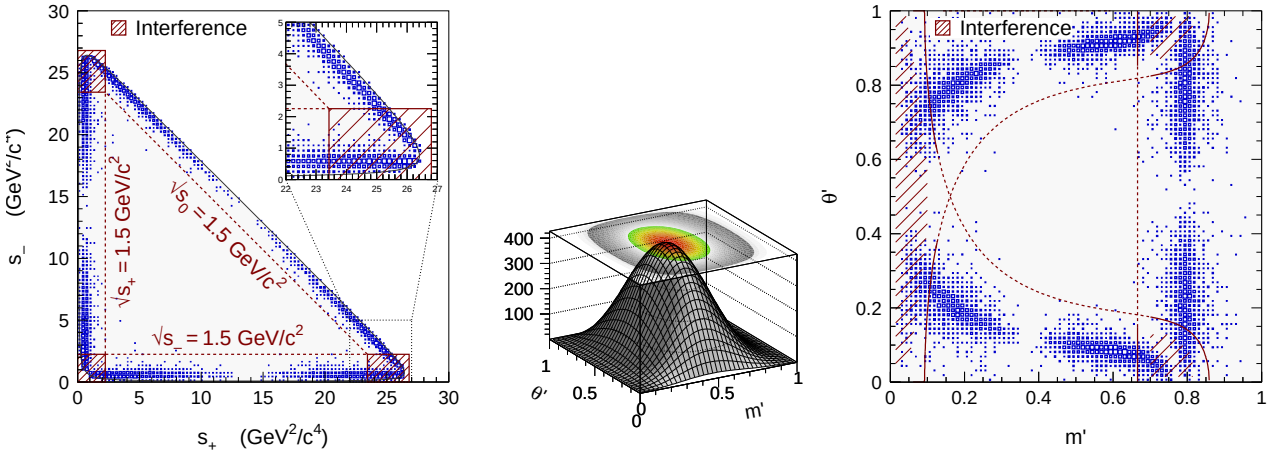

Figure 1: Nominal (left) and square (right) $B^0 \to \pi^+\pi^-\pi^0$ Dalitz plots obtained from Monte Carlo generated events without detector simulation. The generating amplitudes used are $A^+ = A^- = A^0 = 1$ so that they interfere destructively at equal ρ masses. The hatched areas indicate the main overlap regions between the different ρ bands. The contour lines in both plots correspond to $\sqrt{s_{+,-,0}} = 1.5$ GeV/c^2. The middle plot depicts the Jacobian determinant (17) of the transformation (15). The plot shows the distribution one would obtain in the square Dalitz plot for uniformly distributed events in the nominal Dalitz plot.

2 THE *BABAR* DETECTOR AND DATASET

The data used in this analysis were collected with the *BABAR* detector at the PEP-II asymmetric-energy e^+e^- storage ring at SLAC between October 1999 and July 2004. The sample consists of about 192 fb^{-1}, corresponding to $(213.1\pm2.3)\times10^6$ $B\overline{B}$ pairs collected at the $\Upsilon(4S)$ resonance ("on-resonance"), and an integrated luminosity of 11.6 fb^{-1} collected about 40 MeV below the $\Upsilon(4S)$ ("off-resonance").

A detailed description of the *BABAR* detector is presented in Ref. [17]. The tracking system used for track and vertex reconstruction has two main components: a silicon vertex tracker (SVT) and a drift chamber (DCH), both operating within a 1.5 T magnetic field generated by a superconducting solenoidal magnet. Photons are identified in an electromagnetic calorimeter (EMC) surrounding a detector of internally reflected Cherenkov light (DIRC), which associates Cherenkov photons with tracks for particle identification (PID). Muon candidates are identified with the use of the instrumented flux return (IFR) of the solenoid.

3 ANALYSIS METHOD

The U and I coefficients and the $B^0 \to \pi^+\pi^-\pi^0$ event yield are determined by a maximum-likelihood fit of the signal model to the selected candidate events. Kinematic and event shape variables exploiting the characteristic properties of the events are used in the fit to discriminate signal from background. We limit the size of the data sample that enters the fit by tightening the acceptance requirements for the discriminant variables compared to similar analyses, because the fit model with at least 17 physical parameters is rather involved. With the same goal and because the modeling of the distribution of the continuum events in the Dalitz plot is delicate, we remove

the center of the Dalitz plot from the analysis. This requirement does not affect the signal.

3.1 EVENT SELECTION AND BACKGROUND SUPPRESSION

We reconstruct $B^0 \to \pi^+\pi^-\pi^0$ candidates from pairs of oppositely-charged tracks, forming a good quality vertex, and a π^0 candidate. We use information from the tracking system, EMC, and DIRC to remove tracks for which the PID is consistent with the electron, kaon, or proton hypotheses. In addition, we require that at least one track has a signature in the IFR that is inconsistent with the muon hypothesis. The π^0 candidate mass must satisfy $0.11 < m(\gamma\gamma) < 0.16\,\mathrm{GeV}/c^2$, where each photon is required to have an energy greater than 50 MeV in the laboratory frame (LAB) and to exhibit a lateral profile of energy deposition in the EMC consistent with an electromagnetic shower.

Two requirements are applied on the Dalitz plot. Firstly, the invariant mass of the two tracks m_0 must be larger than $0.52\,\mathrm{GeV}/c^2$. This rejects about 80% of the $B^0 \to K^0_S(\to \pi^+\pi^-)\pi^0$ background events, which due to the long lifetime of the K^0_S would require a dedicated Δt treatment. This cut retains 98% (100%) of signal $B^0 \to \rho^0\pi^0$ ($B^0 \to \rho^\pm\pi^\mp$) events. Secondly, we remove the center of the Dalitz plot by requiring that at least one of the three invariant masses, m_0, m_+ or m_-, is lower than 1.5 $\mathrm{GeV/c^2}$.

A B-meson candidate is characterized kinematically by the energy-substituted mass $m_{\rm ES} = [(\frac{1}{2}s + \mathbf{p}_0\cdot\mathbf{p}_B)^2/E_0^2 - \mathbf{p}_B^2]^{\frac{1}{2}}$ and energy difference $\Delta E = E_B^* - \frac{1}{2}\sqrt{s}$, where $(E_B, \mathbf{p}_B)$ and $(E_0, \mathbf{p}_0)$ are the four-vectors of the B-candidate and the initial electron-positron system, respectively. The asterisk denotes the $\Upsilon(4S)$ frame, and s is the square of the invariant mass of the electron-positron system. We require $5.272 < m_{\rm ES} < 5.288\,\mathrm{GeV}/c^2$, which retains 81% of the signal and 8% of the continuum background events. The ΔE resolution exhibits a dependence on the π^0 energy and therefore varies across the Dalitz plot. We account for this effect by introducing the transformed quantity $\Delta E' = (2\Delta E - \Delta E_+ - \Delta E_-)/(\Delta E_+ - \Delta E_-)$, with $\Delta E_\pm(m_0) = c_\pm - (c_\pm \mp \bar{c})\,(m_0/m_0^{\rm max})^2$, where m_0 monitors the π^0-energy dependence. We use the values $\bar{c} = 0.045\,\mathrm{GeV}$, $c_- = -0.140\,\mathrm{GeV}$, $c_+ = 0.080\,\mathrm{GeV}$, $m_0^{\rm max} = 5.0\,\mathrm{GeV}$, and require $-1 < \Delta E' < 1$. These settings have been obtained from Monte Carlo (MC) simulation and are tuned to maximize the selection of correctly reconstructed over misreconstructed signal events. The cut retains 75% (25%) of the signal (continuum).

Backgrounds arise primarily from random combinations in continuum events. To enhance discrimination between signal and continuum, we use a neural network (NN) to combine four discriminating variables: the angles with respect to the beam axis of the B momentum and B thrust axis in the $\Upsilon(4S)$ frame, and the zeroth and second order monomials $L_{0,2}$ of the energy flow about the B thrust axis. The monomials are defined by $L_j = \sum_i p_i \times |\cos\theta_i|^j$, where θ_i is the angle with respect to the B thrust axis of track or neutral cluster i, p_i is its momentum, and the sum excludes the B candidate. The NN is trained in the signal region with off-resonance data and simulated signal events. The final sample of signal candidates is selected with a cut on the NN output that retains 77% (8%) of the signal (continuum).

The time difference Δt is obtained from the measured distance between the z positions (along the beam direction) of the $B^0_{3\pi}$ and $B^0_{\rm tag}$ decay vertices, and the boost $\beta\gamma = 0.56$ of the e^+e^- system[8]. To determine the flavor of the $B^0_{\rm tag}$ we use the tagging algorithm of Ref. [18]. This produces four mutually exclusive tagging categories. We also retain untagged events in a fifth category to improve the efficiency of the signal selection and because these events contribute to the measurement of direct *CP* violation. Events with multiple B candidates passing the full selection

[8] Δt is defined as: $\Delta t = \Delta z/\beta\gamma c$

occur in 16% ($\rho^{\pm}\pi^{\mp}$) and 9% ($\rho^0\pi^0$) of the cases. If the multiple candidates have different π^0's, we choose the candidate with the reconstructed π^0 mass closest to the nominal one; if not, one candidate is selected at random.

The signal efficiency determined from MC simulation is 24% for $B^0 \to \rho^{\pm}\pi^{\mp}$ and $B^0 \to \rho^0\pi^0$ events, and 11% for non-resonant $B^0 \to \pi^+\pi^-\pi^0$ events.

Of the selected signal events, 22% ($B^0 \to \rho^{\pm}\pi^{\mp}$), 13% ($B^0 \to \rho^0\pi^0$), and 6% (non-resonant) are misreconstructed, mostly due to combinatorial background from low-momentum tracks and photons. They concentrate in the corners of the Dalitz plot. The fraction of misreconstructed events strongly varies across the tagging categories.

3.2 BACKGROUND FROM OTHER B DECAYS

We use MC-simulated events to study the background from other B decays. The exclusive B-background modes are grouped into eighteen classes with similar kinematic and topological properties. More than hundred decay channels have been considered of which thirty-six are retained in the likelihood model. The most significant ones are $B^+ \to \rho^+\rho^0$ with longitudinal polarization (27 ± 18 events expected), $B^+ \to \pi^+\rho^0$ (48 ± 6), $B^+ \to \pi^0\rho^+$ (43 ± 7), $B^0 \to \rho^+\rho^-$ with longitudinal polarization (50 ± 10), $B^0 \to (a_1\pi)^0$ (29 ± 11), $B^0 \to \rho^- K^+$ (61 ± 11), and $B^0 \to$ higher kaon resonances (6 ± 1). The charmed modes $B^0 \to D^-(\to \pi^-\pi^0)\pi^+$ and $B^0 \to \overline{D}^0(\to \pi^+\pi^-)\pi^0$ contribute to the selected data sample and are considered in individual classes. They do not interfere with the signal due to the long D lifetime. We also assign classes to the modes $B^0 \to \overline{D}^0(\to K^+\pi^-)\pi^0$ and $B^0 \to J/\psi(\to \ell^+\ell^-)\pi^0$. In total we expect 49 ± 15 exclusive $b \to c$ events. Two additional classes account for inclusive neutral and charged $b \to c$ decays, where we expect 82 ± 6 and 181 ± 9 events, respectively.

3.3 THE MAXIMUM-LIKELIHOOD FIT

We perform an unbinned extended maximum-likelihood fit to extract the inclusive $B^0 \to \pi^+\pi^-\pi^0$ event yield and the U and I coefficients defined in Eqs. (8)–(12). The fit uses the variables $m_{\rm ES}$, $\Delta E'$, the NN output, and the Dalitz plot to discriminate signal from background. The Δt measurement allows to determine mixing-induced CP violation and provides additional continuum-background rejection.

The selected on-resonance data sample is assumed to consist of signal, continuum-background and B-background components, separated by the flavor and tagging category of the tag side B decay. The signal likelihood consists of the sum of a correctly reconstructed ("truth-matched", TM) component and a misreconstructed ("self-cross-feed", SCF) component.

The probability density function (PDF) $\mathcal{P}_i^c$ for an event i in tagging category c is the sum of the probability densities of all components, namely

$$\begin{aligned}
\mathcal{P}_i^c \;\equiv\; & N_{3\pi} f_{3\pi}^c \left[(1 - \overline{f}_{\rm SCF}^c)\mathcal{P}_{3\pi-{\rm TM},i}^c + \overline{f}_{\rm SCF}^c \mathcal{P}_{3\pi-{\rm SCF},i}^c \right] \\
& + N_{q\bar{q}}^c \frac{1}{2} \left(1 + q_{{\rm tag},i} A_{q\bar{q},\,{\rm tag}}\right) \mathcal{P}_{q\bar{q},i}^c \\
& + \sum_{j=1}^{N_{\rm class}^{B^+}} N_{B^+ j} f_{B^+ j}^c \frac{1}{2} \left(1 + q_{{\rm tag},i} A_{B^+,\,{\rm tag},j}\right) \mathcal{P}_{B^+,ij}^c
\end{aligned}$$

$$+ \sum_{j=1}^{N^{B^0}_{\rm class}} N_{B^0 j} f^c_{B^0 j} \mathcal{P}^c_{B^0,ij} \ , \tag{18}$$

where: $N_{3\pi}$ is the total number of $\pi^+\pi^-\pi^0$ signal events the data sample; $f^c_{3\pi}$ is the fraction of signal events that are tagged in category c; $\overline{f}^c_{\rm SCF}$ is the fraction of SCF events in tagging category c, averaged over the Dalitz plot; $\mathcal{P}^c_{3\pi-{\rm TM},i}$ and $\mathcal{P}^c_{3\pi-{\rm SCF},i}$ are the products of PDFs of the discriminating variables used in tagging category c for TM and SCF events, respectively; $N^c_{q\bar{q}}$ is the number of continuum events that are tagged in category c; $q_{{\rm tag},i}$ is the tag flavor of the event, defined to be $+1$ for a $B^0_{\rm tag}$ and -1 for a $\overline{B}^0_{\rm tag}$; $A_{q\bar{q},\,{\rm tag}}$ parameterizes possible tag asymmetry in continuum events; $\mathcal{P}^c_{q\bar{q},i}$ is the continuum PDF for tagging category c; $N^{B^+}_{\rm class}$ ($N^{B^0}_{\rm class}$) is the number of charged (neutral) B-related background classes considered in the fit; $N_{B^+ j}$ ($N_{B^0 j}$) is the number of expected events in the charged (neutral) B-background class j; $f^c_{B^+ j}$ ($f^c_{B^0 j}$) is the fraction of charged (neutral) B-background events of class j that are tagged in category c; $A_{B^+,\,{\rm tag},j}$ describes a possible tag asymmetry in the charged-B background class j; correlations between the tag and the position in the Dalitz plot (the "charge") are absorbed in tag-flavor-dependent Dalitz plot PDFs that are used for charged-B and continuum background; $\mathcal{P}^c_{B^+,ij}$ is the B^+-background PDF for tagging category c and class j; finally, $\mathcal{P}^c_{B^0,ij}$ is the neutral-B-background PDF for tagging category c and class j.

The PDFs $\mathcal{P}^c_X$ are the product of the four PDFs of the discriminating variables, $x_1 = m_{ES}$, $x_2 = \Delta E'$, $x_3 =$ NNoutput, and the triplet $x_4 = \{m', \theta', \Delta t\}$:

$$\mathcal{P}^c_{X,i(j)} \ \equiv \ \prod_{k=1}^{4} P^c_{X,i(j)}(x_k) \ . \tag{19}$$

The extended likelihood over all tagging categories is given by

$$\mathcal{L} \ \equiv \ \prod_{c=1}^{5} e^{-\overline{N}^c} \prod_{i}^{N^c} \mathcal{P}^c_i \ , \tag{20}$$

where $\overline{N}^c$ is the total number of events expected in category c.

A total of 39 parameters, including the inclusive signal yield and the parameters from Eq. (6), are varied in the fit.

3.3.1 THE Δt AND DALITZ PLOT PDFS

Signal Parameterization. The Dalitz plot PDFs require as input the Dalitz plot-dependent relative selection efficiency, $\epsilon = \epsilon(m', \theta')$, and SCF fraction, $f_{\rm SCF} = f_{\rm SCF}(m', \theta')$. Both quantities are taken from MC simulation. They are given in Fig. 2 (left plot for ϵ and right plot for $f_{\rm SCF}$), where the symmetry of the Dalitz plot has been used to fold the upper θ' half into the lower one. Away from the Dalitz plot corners the efficiency is uniform, while it decreases when approaching the corners, where one out of the three bodies in the final state is close to rest so that the acceptance requirements on the particle reconstruction become incisive. Combinatorial backgrounds and hence SCF fractions are large in the corners of the Dalitz plot due to the presence of soft neutral clusters and tracks.

For an event i, we define the time-dependent Dalitz plot PDFs

$$P_{3\pi-{\rm TM},i} \ = \ \varepsilon_i \, (1 - f_{{\rm SCF},i}) \, |\det J_i| \, |\mathcal{A}^{\pm}_{3\pi}(\Delta t)|^2 \ , \tag{21}$$

$$P_{3\pi-{\rm SCF},\,i} \ = \ \varepsilon_i \, f_{{\rm SCF},i} \, |\det J_i| \, |\mathcal{A}^{\pm}_{3\pi}(\Delta t)|^2 \ , \tag{22}$$

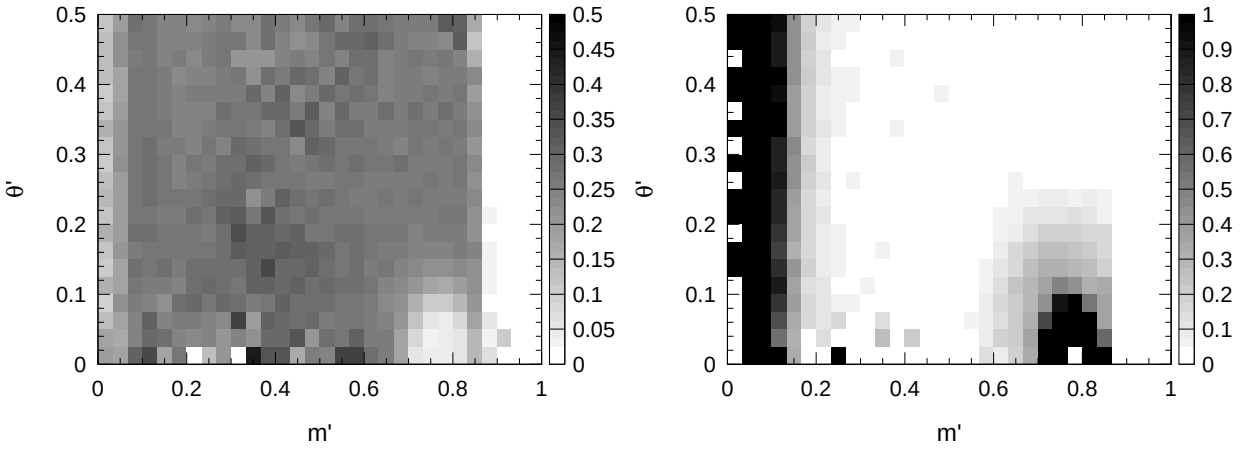

Figure 2: Selection efficiency of $B^0 \to \pi^+\pi^-\pi^0$ events (left) and fraction of misreconstructed events (right) in the (symmetrized) square Dalitz plot for MC-simulated events.

where $P_{3\pi-\mathrm{TM},i}$ and $P_{3\pi-\mathrm{SCF},i}$ are normalized. The corresponding phase space integration involves the expectation values $\langle \varepsilon\,(1-f_{\mathrm{SCF}})\,|\det J|\,f^\kappa f^{\sigma *}\rangle$ and $\langle \varepsilon\, f_{\mathrm{SCF}}\,|\det J|\,f^\kappa f^{\sigma *}\rangle$ for TM and SCF events, where the indices κ, σ run over all resonances belonging to the signal model. The expectation values are model-dependent and are computed with the use of MC integration over the square Dalitz plot:

$$\langle \varepsilon\,(1-f_{\mathrm{SCF}})\,|\det J|\,f^\kappa f^{\sigma *}\rangle \;=\; \frac{\int_0^1\int_0^1 \varepsilon\,(1-f_{\mathrm{SCF}})\,|\det J|\,f^\kappa f^{\sigma *}\,dm'd\theta'}{\int_0^1\int_0^1 \varepsilon\,|\det J|\,f^\kappa f^{\sigma *}\,dm'd\theta'}\;, \tag{23}$$

and similarly for $\langle \varepsilon\;|\det J|\,f^\kappa f^{\sigma *}\rangle$, where all quantities in the integrands are Dalitz plot-dependent.

Equation (18) invokes the phase space-averaged SCF fraction $\overline{f}_{\mathrm{SCF}} \equiv \langle f_{\mathrm{SCF}}\,|\det J|\,f^\kappa f^{\sigma *}\rangle$. As for the PDF normalization, it is decay-dynamics-dependent. It has to be computed iteratively, though the remaining systematic uncertainty after one iteration step is small. We determine the average SCF fractions separately for each tagging category from MC simulation.

The width of the dominant $\rho(770)$ resonance is large compared to the mass resolution for TM events (about $8\,\mathrm{MeV}/c^2$ core Gaussian resolution). We can therefore neglect resolution effects in the TM model. Misreconstructed events have a poor mass resolution that strongly varies across the Dalitz plot. It is described in the fit by a 2×2-dimensional resolution function

$$R_{\mathrm{SCF}}(m'_r,\theta'_r,m'_t,\theta'_t)\;, \tag{24}$$

which represents the probability to reconstruct at the coordinate (m'_r,θ'_r) an event that has the true coordinate (m'_t,θ'_t). It obeys the unitarity condition

$$\int\limits_0^1\int\limits_0^1 R_{\mathrm{SCF}}(m'_r,\theta'_r,m'_t,\theta'_t)\,dm'_r d\theta'_r \;=\; 1\;,\quad \forall\,(m'_t,\theta'_t)\in \mathrm{SDP}\;, \tag{25}$$

and is convolved with the signal model. The R_{SCF} function is obtained from MC simulation. Figure 3 shows the resolution function of TM (left) and SCF events (right) for two coordinates depicted by the open stars.

We use the signal model described in Section 1.1. It contains the dynamical information and is connected with Δt via the matrix element (6), which serves as PDF. It is diluted by the effects

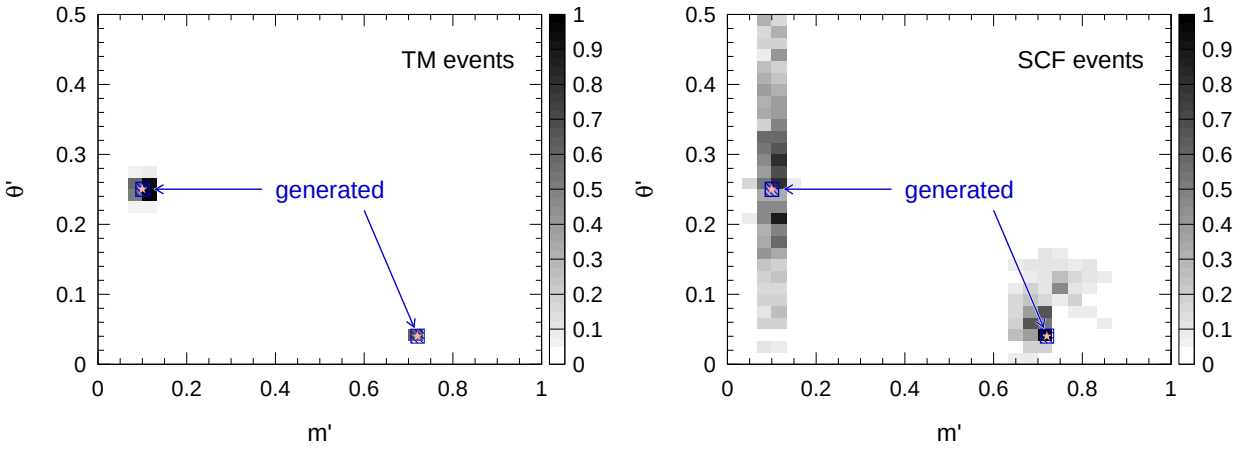

Figure 3: Resolution for TM (left) and SCF events (right hand plot) in the square Dalitz plot for two coordinates indicated by the open stars.

of mistagging and the limited vertex resolution [10]. The Δt resolution function for signal and B-background events is a sum of three Gaussian distributions, with parameters determined by a fit to fully reconstructed B^0 decays [18].

Background Parameterization. The Dalitz plot- and Δt-dependent PDFs factorize for the charged-B-background modes, but not (necessarily) for the neutral-B background due to $B^0\overline{B}^0$ mixing.

The charged B-background contribution to the likelihood (18) invokes the parameter $A_{B^+,\mathrm{tag}}$, multiplied by the tag flavor q_{tag} of the event. In the presence of significant tag-"charge" correlation (represented by an effective flavor-tag-versus-Dalitz-coordinate correlation), it parameterizes possible direct CP violation in these events. We also use distinct square Dalitz plot PDFs for each reconstructed B flavor tag, and a flavor-tag-averaged PDF for untagged events. The PDFs are obtained from MC simulation and are described with the use of non-parametric functions. The Δt resolution parameters are determined by a fit to fully reconstructed B^+ decays. For each B^+-background class we adjust effective lifetimes to account for the misreconstruction of the event that modifies the nominal Δt resolution function.

The neutral-B background is parameterized with PDFs that depend on the flavor tag of the event. In the case of CP eigenstates, correlations between the flavor tag and the Dalitz coordinate are expected to be small. However, non-CP eigenstates, such as $a_1^{\pm}\pi^{\mp}$, may exhibit such correlation. Both types of decays can have direct and mixing-induced CP violation. A third type of decays involves charged kaons and does not exhibit mixing-induced CP violation, but usually has a strong correlation between the flavor tag and the Dalitz plot coordinate (the kaon charge), because it consists of B-flavor eigenstates. The Dalitz plot PDFs are obtained from MC simulation and are described with the use of non-parametric functions. For neutral B background, the signal Δt resolution model is assumed.

The Dalitz plot treatment of the continuum events is similar to the one used for charged-B background. The square Dalitz plot PDF for continuum background is obtained from on-resonance events selected in the m_{ES} sidebands and corrected for feed-through from B decays. A large number of cross checks has been performed to ensure the high fidelity of the empirical shape parameterization. Analytical models have been found insufficient. The continuum Δt distribution

is parameterized as the sum of three Gaussian distributions with common mean and three distinct widths that scale the Δt per-event error. This yields six shape parameters that are determined by the fit. The model is motivated by the observation that the Δt average is independent of its error, and that the Δt RMS depends linearly on the Δt error.

3.3.2 PARAMETERIZATION OF THE OTHER VARIABLES

The $m_{\rm ES}$ distribution of TM signal events is parameterized by a bifurcated Crystal Ball function [20], which is a combination of a one-sided Gaussian and a Crystal Ball function. The mean of this function is determined by the fit. A non-parametric function is used to describe the SCF signal component.

The $\Delta E'$ distribution of TM events is parameterized by a double Gaussian function, where all five parameters depend linearly on m_0^2. Misreconstructed events are parameterized by a broad single Gaussian function.

Both $m_{\rm ES}$ and $\Delta E'$ PDFs are parameterized by non-parametric functions for all B-background classes.

The $m_{\rm ES}$ and $\Delta E'$ PDFs for continuum events are parameterized with an Argus shape function [21] and a second order polynomial, respectively, with parameters determined by the fit.

We use non-parametric functions to empirically describe the distributions of the NN outputs found in the MC simulation for TM and SCF signal events, and for B-background events. We distinguish tagging categories for TM signal events to account for differences observed in the shapes.

The continuum NN distribution is parameterized by a third order polynomial that is defined to be positive. The coefficients of the polynomial are determined by the fit. Continuum events exhibit a correlation between the Dalitz plot coordinate and the shape of the event that is exploited in the NN. The tight requirement that eliminates the center of the Dalitz plot has the purpose to reduce such correlation. To correct for residual effects, we introduce a linear dependence of the polynomial coefficients on the distance of the Dalitz plot coordinate to the kinematic boundaries of the Dalitz plot. The parameters describing this dependence are determined by the fit.

4 SYSTEMATIC STUDIES

The contributions to the systematic error on the signal parameters are summarized in Table 1.

The uncertainties associated with Δm_d and τ are estimated by varying these parameters within the uncertainties on the world average [19].

The systematic effects due to the signal PDFs ("Signal description" field in Table 1) comprise uncertainties in the PDF parameterization, the treatment of misreconstructed events, the tagging performance, and the modeling of the signal contributions.

When the signal PDFs are determined from fits to a control sample of fully reconstructed B decays to exclusive final states with charm, the uncertainties are obtained by varying the parameters within the statistical uncertainties. In other cases, the dominant parameters have been left free to vary in the fit, and the differences observed in these fits are taken as systematic errors.

The average fraction of misreconstructed signal events predicted by the MC simulation has been verified with fully reconstructed $B \to D\rho$ events [10]. No significant differences between data and the simulation were found. We vary $\overline{f}_{\rm SCF}$ for all tagging categories by relative 25% to estimate the systematic uncertainty (contained in "Signal description" in Table 1).

	I_-	I_+	U_0^+	U_-^-	U_-^+	U_+^-	$U_{+-}^{-,\mathrm{Im}}$	$U_{+-}^{-,\mathrm{Re}}$
Δm_d and τ_{B^0}	0.003	0.001	0.000	0.004	0.000	0.001	0.003	0.007
Signal description	0.005	0.004	0.001	0.011	0.013	0.010	0.042	0.056
Tagging	0.003	0.002	0.001	0.010	0.001	0.010	0.042	0.019
Signal model	0.004	0.005	0.011	0.013	0.004	0.020	0.202	0.154
B Background	0.011	0.013	0.007	0.029	0.015	0.035	0.118	0.071
Continuum parametrization	0.004	0.004	0.040	0.002	0.012	0.004	0.027	0.031
Fixing 10 $\rho^0\pi^0$ parameters	0.003	0.003	0.025	0.019	0.007	0.039	0.042	0.022
Fit Bias	0.015	0.014	0.006	0.022	0.015	0.020	0.177	0.161
Sum	0.021	0.021	0.050	0.046	0.029	0.061	0.303	0.244

	$U_{+-}^{+,\mathrm{Im}}$	$U_{+-}^{+,\mathrm{Re}}$	I_{+-}^{Im}	I_{+-}^{Re}	$U_{+0}^{+,\mathrm{Im}}$	$U_{+0}^{+,\mathrm{Re}}$	$U_{-0}^{+,\mathrm{Im}}$	$U_{-0}^{+,\mathrm{Re}}$
Δm_d and τ_{B^0}	0.002	0.001	0.010	0.041	0.001	0.001	0.001	0.001
Signal description	0.014	0.043	0.108	0.063	0.013	0.029	0.048	0.016
Tagging	0.009	0.011	0.062	0.041	0.004	0.006	0.005	0.007
Signal model	0.079	0.137	0.629	0.333	0.129	0.096	0.107	0.161
B Background	0.065	0.038	0.159	0.179	0.012	0.040	0.038	0.038
Continuum parametrization	0.031	0.034	0.097	0.099	0.019	0.059	0.012	0.028
Fixing 10 $\rho^0\pi^0$ parameters	0.019	0.010	0.024	0.004	0.110	0.069	0.102	0.000
Fit Bias	0.078	0.076	0.221	0.240	0.051	0.048	0.055	0.047
Sum	0.135	0.171	0.704	0.467	0.179	0.149	0.170	0.175

Table 1: Summary of systematic uncertainties.

Tagging efficiencies, dilutions and biases for signal events are varied within their experimental uncertainties.

The most important contribution to the systematic uncertainty stems from the signal modeling of the Dalitz plot dynamics. We vary the mass and width of the $\rho(770)$ and $\rho(1450)$ within ranges that exceed twice the errors found for these parameters in the fits to τ and e^+e^- data [11]. Since some of the U and I coefficients exhibit significant dependence on the $\rho(1450)$ contribution, we leave its amplitude (phase and fraction) free to vary in the nominal fit. We vary the relative amount of $\rho(1700)$ by 30% with respect to the nominal model, and its phase by 8°, to assign a systematic error. We have performed a fit where the $\rho(1700)$ amplitude parameters (magnitude and phase) are free to vary. We find results that are in agreement with the nominal model. The variations for the U and I coefficients observed in this fit compared to the nominal one are smaller than the systematic uncertainties we assign due to the $\rho(1700)$ amplitude uncertainty.

To estimate the contribution from non-resonance $B^0 \to \pi^+\pi^-\pi^0$ events, we have performed an independent analysis where we apply the contrary of the Dalitz plot requirement that is used in the nominal analysis; to remove the ρ signal we retain only those events for which the minimum invariant mass exceeds $1.5\,\mathrm{GeV}/c^2$. For simplicity, we assume a uniform Dalitz distribution for the

non-resonance events. The fit finds no non-resonant events so that we can determine a preliminary upper limit of 1.4×10^{-6} at 90% confidence level (statistical errors only). According to this limit, we add simulated non-resonant events to the nominal data sample to estimate the systematic uncertainty. We have also searched for the presence of $B^0 \to f_0(980)\pi^0$ events without finding evidence for a signal.

A major source of systematic uncertainty is the B-background model. The expected event yields from the background modes are varied according to the uncertainties in the measured or estimated branching fractions. Since B-background modes may exhibit *CP* violation, the corresponding parameters are varied within appropriate uncertainty ranges. As is done for the signal PDFs, we vary the Δt resolution parameters and the flavor-tagging parameters within their uncertainties and assign the differences observed in the on-resonance data fit with respect to nominal fit as systematic errors.

The parameters for the continuum events are determined by the fit. No additional systematic uncertainties are assigned to them. An exception to this is the Dalitz plot PDF: to estimate the systematic uncertainty from the $m_{\rm ES}$ sideband extrapolation, we select large samples of off-resonance data by loosening the requirements on ΔE and the NN. We compare the distributions of m' and θ' between the $m_{\rm ES}$ sideband and the signal region. No significant differences are found. We assign as systematic error the effect seen when weighting the continuum Dalitz plot PDF by the ratio of both data sets. This effect is mostly statistical in origin. To account for possible inaccuracies in the empirical parameterization, we add test components with floating event yields to the fit that consist of continuum-background-like reference distributions in all fit variables but the Dalitz plot, for which signal-like distributions are used. In addition, we leave the B-background classes free to vary in the fit. This allows the fit to absorb events that, due to possible problems in the continuum Dalitz plot description, would bias the signal yield. The shifts in the signal parameters observed when adding these test components are taken as systematic uncertainties ("continuum parameterization" in Table 1). It leads to significant effects in the $\rho^0\pi^0$ region of the Dalitz plot.

We assess the dependence of the results on whether all the 27 U and I coefficients are free in the fit or only the 16 most significant ones. To study this effect, we generate MC samples with values for the U and I coefficients according to our nominal 16 parameter fit result. We then perform a full amplitude fit to these 16 coefficients (*cf.* Section 6) and compute from the best fit the expected values for the missing coefficients. Monte Carlo samples are generated with the use of all 27 coefficients, which are fit with the nominal model where 10 coefficients are set to zero. The observed systematic effect on the measured U and I coefficients depend on the branching fraction for $B^0 \to \rho^0\pi^0$ for which we use our upper bound [22] (which is in agreement with the finding in this analysis).

Finally, to validate the fitting tool, we perform fits on large MC samples with the measured proportions of signal, continuum and B-background events. No significant biases are observed in these fits. The statistical uncertainties on the fit parameters are taken as systematic uncertainties ("Fit bias").

The systematic errors for the parameters that measure interference effects are dominated by the uncertainty in the signal model, mainly the tail description of the ρ resonance. For the other parameters, the uncertainty on the fit bias and the B-background contamination are important.

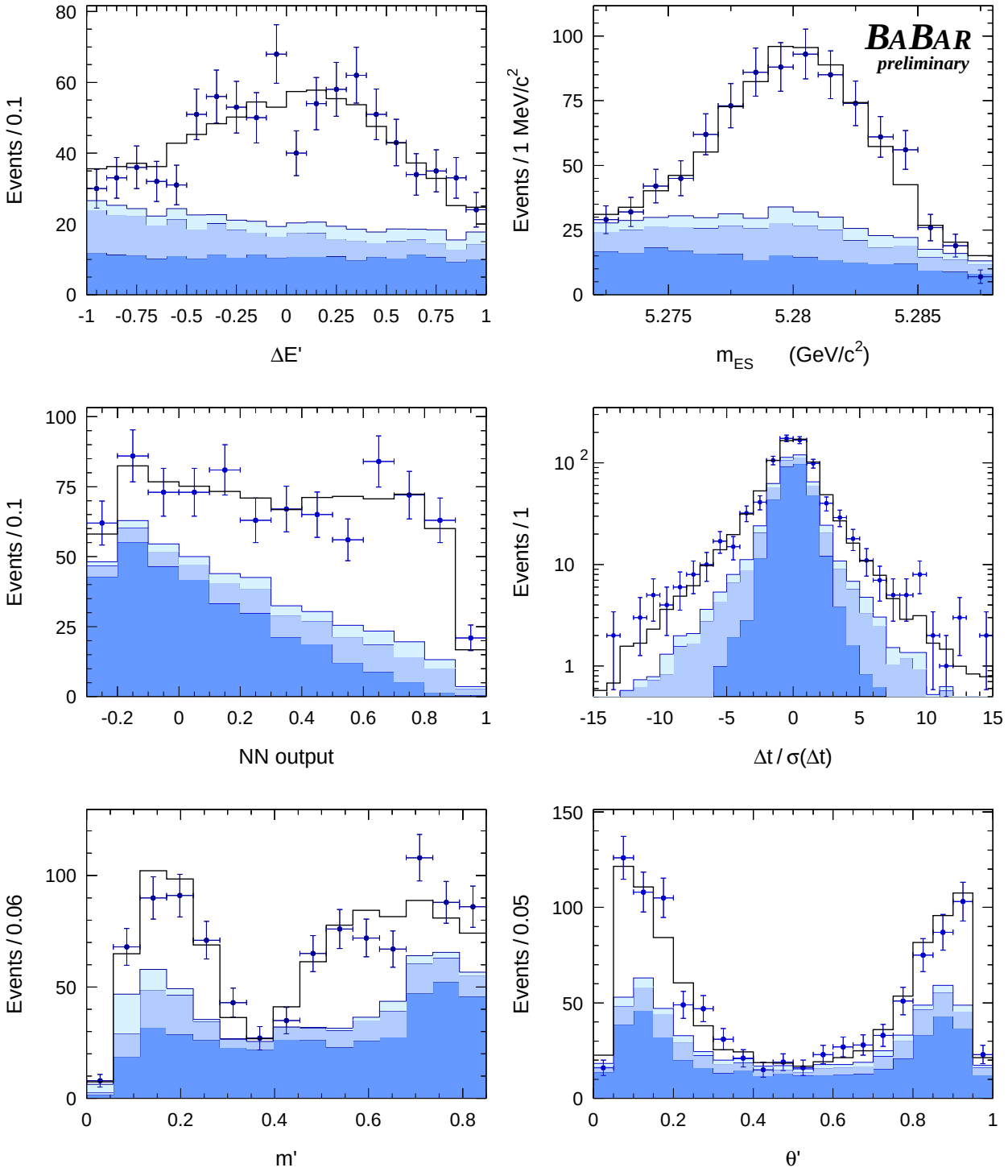

Figure 4: Distributions of (clockwise from top left) $\Delta E'$, $m_{\rm ES}$, NN output, $\Delta t/\sigma(\Delta t)$, m' and θ' for samples enhanced in $B^0 \to \pi^+\pi^-\pi^0$ signal. The dots with error bars give the on-resonance data. The solid histogram shows the projection of the fit result. The dark, medium and light shaded areas represent respectively the contribution from continuum events, the sum of continuum events and the B-background expectation, and the sum of these and the misreconstructed signal events.

Parameter	Description	Result
I_-	Coefficient of $\lvert f_-\rvert^2 \sin(\Delta m_d \Delta t)$	$-0.19 \pm 0.11 \pm 0.02$
I_+	Coefficient of $\lvert f_+\rvert^2 \sin(\Delta m_d \Delta t)$	$0.06 \pm 0.11 \pm 0.02$
U_0^+	Coefficient of $\lvert f_0\rvert^2$	$0.16 \pm 0.05 \pm 0.05$
U_-^-	Coefficient of $\lvert f_-\rvert^2 \cos(\Delta m_d \Delta t)$	$0.22 \pm 0.16 \pm 0.05$
U_-^+	Coefficient of $\lvert f_-\rvert^2$	$1.19 \pm 0.12 \pm 0.03$
U_+^-	Coefficient of $\lvert f_+\rvert^2 \cos(\Delta m_d \Delta t)$	$0.50 \pm 0.17 \pm 0.06$
$U_{+-}^{-,\mathrm{Im}}$	Coefficient of $\mathrm{Im}[f_+ f_-^*] \cos(\Delta m_d \Delta t)$	$0.3 \pm 1.4 \pm 0.3$
$U_{+-}^{-,\mathrm{Re}}$	Coefficient of $\mathrm{Re}[f_+ f_-^*] \cos(\Delta m_d \Delta t)$	$2.0 \pm 1.2 \pm 0.2$
$U_{+-}^{+,\mathrm{Im}}$	Coefficient of $\mathrm{Im}[f_+ f_-^*]$	$0.16 \pm 0.70 \pm 0.14$
$U_{+-}^{+,\mathrm{Re}}$	Coefficient of $\mathrm{Re}[f_+ f_-^*]$	$-0.26 \pm 0.65 \pm 0.17$
I_{+-}^{Im}	Coefficient of $\mathrm{Im}[f_+ f_-^*] \sin(\Delta m_d \Delta t)$	$-5.2 \pm 1.9 \pm 0.7$
I_{+-}^{Re}	Coefficient of $\mathrm{Re}[f_+ f_-^*] \sin(\Delta m_d \Delta t)$	$-0.3 \pm 2.0 \pm 0.5$
$U_{+0}^{+,\mathrm{Im}}$	Coefficient of $\mathrm{Im}[f_+ f_0^*]$	$0.25 \pm 0.35 \pm 0.18$
$U_{+0}^{+,\mathrm{Re}}$	Coefficient of $\mathrm{Re}[f_+ f_0^*]$	$-0.34 \pm 0.39 \pm 0.15$
$U_{-0}^{+,\mathrm{Im}}$	Coefficient of $\mathrm{Im}[f_- f_0^*]$	$0.34 \pm 0.43 \pm 0.17$
$U_{-0}^{+,\mathrm{Re}}$	Coefficient of $\mathrm{Re}[f_- f_0^*]$	$-0.98 \pm 0.44 \pm 0.18$

Table 2: Fit results for the U and I coefficients. The errors given are statistical (first) and systematic (second). The free normalization parameter U_+^+ is fixed to 1.

5 FIT RESULTS

The maximum-likelihood fit results in the $B^0 \to \pi^+\pi^-\pi^0$ event yield 1184 ± 58, where the error is statistical only. For the U and I coefficients we find the results given together with their statistical and systematic errors in Table 2. The corresponding correlation matrix is given in Table 3. We have generated a sample of Monte Carlo experiments to determine the probability density distributions of the fit parameters. Within the statistical uncertainties of this sample we find symmetric pulls and root-mean-squares of order of unity for the U and I coefficients. This allows us to use the least-squares method to derive other quantities from these (Section 6).

The signal is dominated by $B^0 \to \rho^\pm\pi^\mp$ decays. We observe an excess of $\rho^0\pi^0$ events, which is in agreement with our previous upper limit of 2.9×10^{-6} at 90% C.L. [22]. The result for the $\rho(1450)$ amplitude is in agreement with the findings in τ and e^+e^- decays [11]. For the relative strong phase between the $\rho(770)$ and the $\rho(1450)$ amplitudes we find $(199\,^{+13}_{-17})^\circ$ (statistical error only), which is compatible with the result from τ and e^+e^- data.

Figure 4 shows distributions of $\Delta E'$, m_{ES}, the NN output, $\Delta t/\sigma(\Delta t)$, where $\sigma(\Delta t)$ is the per-event error on Δt, as well as the Dalitz plot variables m' and θ', which are enhanced in signal content by cuts on the signal-to-continuum likelihood ratios of the other discriminating variables.

As a validation of our treatment of the time dependence we allow τ_{B^0} and Δm_d to vary in the fit. We find $\tau_{B^0} = (1.549 \pm 0.080)\,\mathrm{ps}$ and $\Delta m_d = (0.57 \pm 0.11)\,\mathrm{ps}^{-1}$, while the remaining free parameters are consistent with the nominal fit. To validate the SCF modeling, we let the average SCF fractions per tagging category free to vary in the fit and find results that are consistent with

	I_-	I_+	U_0^+	U_-^-	U_-^+	U_+^-	$U_{+-}^{-,\mathrm{Im}}$	$U_{+-}^{-,\mathrm{Re}}$	$U_{+-}^{+,\mathrm{Im}}$	$U_{+-}^{+,\mathrm{Re}}$	I_{+-}^{Im}	I_{+-}^{Re}	$U_{+0}^{+,\mathrm{Im}}$	$U_{+0}^{+,\mathrm{Re}}$	$U_{-0}^{+,\mathrm{Im}}$
I_-	1.00														
I_+	0.00	1.00													
U_0^+	0.16	0.21	1.00												
U_-^-	0.03	0.01	0.01	1.00											
U_-^+	0.01	0.01	−0.05	0.00	1.00										
U_+^-	−0.06	−0.03	0.01	−0.03	−0.06	1.00									
$U_{+-}^{-,\mathrm{Im}}$	0.07	−0.04	0.07	−0.10	−0.05	−0.04	1.00								
$U_{+-}^{-,\mathrm{Re}}$	−0.02	−0.01	−0.04	0.02	0.01	0.01	−0.05	1.00							
$U_{+-}^{+,\mathrm{Im}}$	−0.10	−0.01	−0.09	0.05	0.13	0.13	−0.05	0.15	1.00						
$U_{+-}^{+,\mathrm{Re}}$	−0.03	0.02	−0.02	0.02	−0.08	0.07	−0.01	−0.01	−0.03	1.00					
I_{+-}^{Im}	0.09	−0.05	0.06	−0.10	0.04	−0.00	0.27	−0.04	−0.14	−0.10	1.00				
I_{+-}^{Re}	−0.02	0.00	0.01	0.06	0.03	−0.02	−0.02	−0.04	0.05	−0.03	−0.01	1.00			
$U_{+0}^{+,\mathrm{Im}}$	−0.07	−0.00	−0.18	0.03	0.03	−0.01	−0.11	0.08	0.06	0.02	−0.10	0.12	1.00		
$U_{+0}^{+,\mathrm{Re}}$	−0.00	−0.01	0.04	−0.19	0.01	0.00	0.13	−0.00	−0.06	−0.04	0.13	0.01	−0.16	1.00	
$U_{-0}^{+,\mathrm{Im}}$	0.02	−0.01	0.13	0.01	−0.05	0.01	0.03	−0.01	−0.04	0.04	0.00	−0.15	−0.19	−0.00	1.00
$U_{-0}^{+,\mathrm{Re}}$	−0.05	−0.05	−0.05	0.01	0.01	0.04	−0.06	0.03	0.13	0.01	−0.07	0.12	0.14	−0.05	−0.01

Table 3: Correlation matrix for the U and I coefficients obtained including statistical and systematic errors.

the MC prediction. We also leave the B-background yields that normalize the B-background classes free to vary for those classes that have sufficiently different distributions of the fit variables to be distinguished from signal. The results are compatible with the model assumptions.

6 INTERPRETATION OF THE RESULTS

The U and I coefficients are related to the quasi-two-body parameters, defined in Ref. [10][9], as follows

$$C^+ = \frac{U_+^-}{U_+^+}\,, \qquad C^- = \frac{U_-^-}{U_-^+}\,, \qquad S^+ = \frac{2\,I_+}{U_+^+}\,, \qquad S^- = \frac{2\,I_-}{U_-^+}\,, \qquad \mathcal{A}_{\rho\pi} = \frac{U_+^+ - U_-^+}{U_+^+ + U_-^+}\,, \tag{26}$$

and where $C = (C^+ + C^-)/2$, $\Delta C = (C^+ - C^-)/2$, $S = (S^+ + S^-)/2$, and $\Delta S = (S^+ - S^-)/2$. In contrast to our previous analysis [10], the definitions of Eq. (26) explicitly account for the presence of interference effects, and are thus exact even for a ρ with finite width, as long as the U and I coefficients are obtained with a Dalitz plot analysis. This treatment leads to a dilution of the result and hence to slightly increased statistical uncertainties compared to neglecting the interference effects.

For the CP-violation parameters, we obtain

$$\mathcal{A}_{\rho\pi} = -0.088 \pm 0.049 \pm 0.013\,, \tag{27}$$

$$C = 0.34 \pm 0.11 \pm 0.05\,, \tag{28}$$

$$S = -0.10 \pm 0.14 \pm 0.04\,, \tag{29}$$

[9]For the cosine coefficients we adopt the convention: $C^+ = [\Gamma(B^0 \to \rho^+\pi^-) - \Gamma(\overline{B}^0 \to \rho^+\pi^-)]/[\Gamma(B^0 \to \rho^+\pi^-) + \Gamma(\overline{B}^0 \to \rho^+\pi^-)]$ and $C^- = [\Gamma(B^0 \to \rho^-\pi^+) - \Gamma(\overline{B}^0 \to \rho^-\pi^+)]/[\Gamma(B^0 \to \rho^-\pi^+) + \Gamma(\overline{B}^0 \to \rho^-\pi^+)]$.

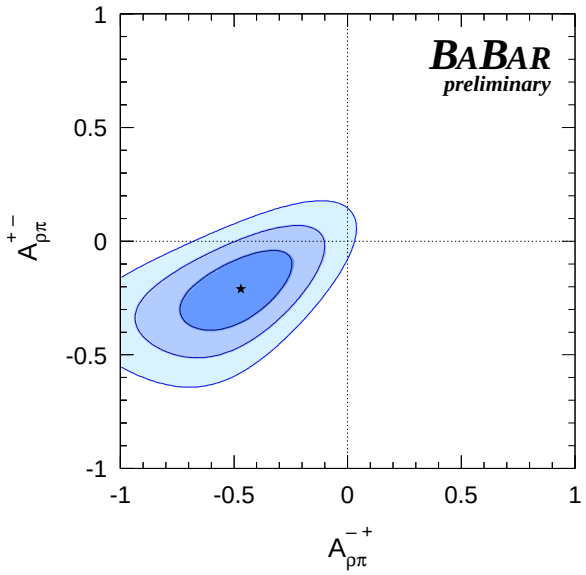

Figure 5: Confidence level contours for the direct *CP* asymmetries $\mathcal{A}^{+-}_{\rho\pi}$ versus $\mathcal{A}^{-+}_{\rho\pi}$. The shaded areas represent 1σ, 2σ and 3σ contours, respectively.

where the first errors given are statistical and the second systematic. For the other parameters in the quasi-two-body description of the $B^0(\overline{B}^0) \to \rho\pi$ decay-time dependence, we measure

$$\Delta C = 0.15 \pm 0.11 \pm 0.03 \ , \tag{30}$$
$$\Delta S = 0.22 \pm 0.15 \pm 0.03 \ . \tag{31}$$

We find the linear correlation coefficients $c_{C,\Delta C} = 0.20$ and $c_{S,\Delta S} = 0.14$, while all other correlations are smaller. The systematic errors are dominated by the uncertainty on the *CP* content of the *B*-related backgrounds. Other contributions are the signal description in the likelihood model (including the limit on non-resonant $B^0 \to \pi^+\pi^-\pi^0$ events), and the fit bias uncertainty.

One can transform the experimentally convenient, namely uncorrelated, direct *CP*-violation parameters C and $\mathcal{A}_{\rho\pi}$ into the physically more intuitive quantities $\mathcal{A}^{+-}_{\rho\pi}$, $\mathcal{A}^{-+}_{\rho\pi}$, defined by

$$\mathcal{A}^{+-}_{\rho\pi} = \frac{|\kappa^{+-}|^2 - 1}{|\kappa^{+-}|^2 + 1} = -\frac{\mathcal{A}_{\rho\pi} + C + \mathcal{A}_{\rho\pi}\Delta C}{1 + \Delta C + \mathcal{A}_{\rho\pi} C} \ , \tag{32}$$
$$\mathcal{A}^{-+}_{\rho\pi} = \frac{|\kappa^{-+}|^2 - 1}{|\kappa^{-+}|^2 + 1} = \frac{\mathcal{A}_{\rho\pi} - C - \mathcal{A}_{\rho\pi}\Delta C}{1 - \Delta C - \mathcal{A}_{\rho\pi} C} \ ,$$

where $\kappa^{+-} = (q/p)(\overline{A}^-/A^+)$ and $\kappa^{-+} = (q/p)(\overline{A}^+/A^-)$, so that $\mathcal{A}^{+-}_{\rho\pi}$ ($\mathcal{A}^{-+}_{\rho\pi}$) involves only diagrams where the ρ (π) meson is emitted by the W boson. We find

$$\mathcal{A}^{+-}_{\rho\pi} = -0.21 \pm 0.11 \pm 0.04 \ , \tag{33}$$
$$\mathcal{A}^{-+}_{\rho\pi} = -0.47\,^{+0.14}_{-0.15} \pm 0.06 \ , \tag{34}$$

with a correlation coefficient of 0.59 between $\mathcal{A}^{+-}_{\rho\pi}$ and $\mathcal{A}^{-+}_{\rho\pi}$. The confidence level contours including systematic errors are given in Fig. 5. The significance, including systematics, for the observation of non-zero direct *CP* violation is at the 2.9σ level.

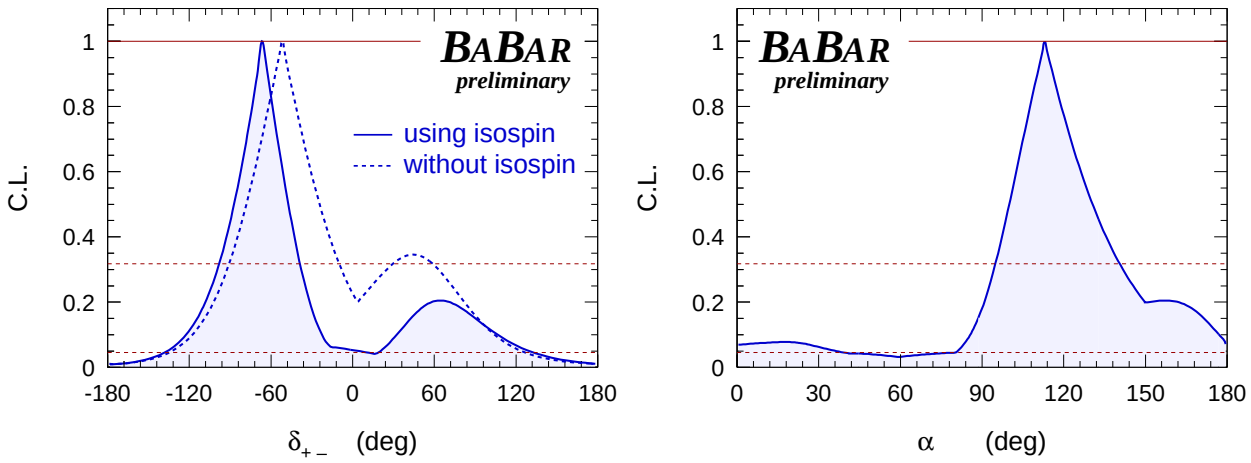

Figure 6: Confidence level functions for δ_{+-} (left) and α (right). Indicated by the dashed horizontal lines are the C.L. values corresponding to 1σ and 2σ, respectively.

The measurement of the resonance interference terms allows us to determine the relative phase

$$\delta_{+-} = \arg\left(A^{+*}A^{-}\right) \ , \tag{35}$$

between the amplitudes of the decays $B^0 \to \rho^-\pi^+$ and $B^0 \to \rho^+\pi^-$. Through the definitions (8)–(12), we can derive a constraint on δ_{+-} from the measured U and I coefficients[10] by performing a least-squares minimization with the six complex amplitudes as free parameters. In this fit, one complex amplitude can be fixed due to an arbitrary global phase and the normalization condition $U_+^+ = 1$, leaving 10 real-valued unknowns. We obtain the confidence level (C.L.) function represented by the dashed line in the left hand plot of Fig. 6. The function includes systematic errors.

This result does not require assumptions beyond the ones outlined in the introduction. The constraint can be improved with the use of strong isospin symmetry. The amplitudes A^κ represent the sum of tree-level and penguin-type amplitudes, which have different CKM factors: the tree-level (T^κ) $B^0 \to \rho^\kappa\pi^{\overline{\kappa}}$ transition amplitude[11] is proportional to $V_{ud}V_{ub}^*$, while the corresponding penguin-type amplitude (P^κ) comes with $V_{qd}V_{qb}^*$, where $q = u, c, t$. Using the unitarity of the CKM matrix one can reorganize the amplitudes and obtains [12]

$$\begin{aligned} A^\kappa &= T^\kappa e^{-i\alpha} + P^\kappa \ , \\ \overline{A}^\kappa &= T^{\overline{\kappa}} e^{+i\alpha} + P^{\overline{\kappa}} \ , \end{aligned} \tag{36}$$

where the magnitudes of the CKM factors have been absorbed in the T^κ, P^κ, $T^{\overline{\kappa}}$ and $P^{\overline{\kappa}}$. The Eqs. (36) represent 13 unknowns of which two can be fixed due to an arbitrary global phase and the normalization condition $U_+^+ = 1$. Using strong isospin symmetry and neglecting isospin-breaking effects, one can identify $P^0 = -(P^+ + P^-)/2$, which reduces the number of unknowns to be determined by the fit to 9. This set of parameters provides the constraint on δ_{+-}, given by the

[10] Using directly the relation $\delta_{+-} = -\arctan\left[\left(U_{+-}^{+,\mathrm{Im}} + U_{+-}^{-,\mathrm{Im}}\right) / \left(U_{+-}^{+,\mathrm{Re}} + U_{+-}^{-,\mathrm{Re}}\right)\right]$ to determine δ_{+-}, leads only to a weak constraint, because it does not include all the available fit information.

[11] We denote by $\overline{\kappa}$ the charge conjugate of κ, where $\overline{0} = 0$.

solid line on the left plot of Fig. 6. The fit returns a minimum χ^2 of 7.4, which has a significance level of 0.39 for 7 degrees of freedom. We find for the solution that is favored by the fit

$$\delta_{+-} \;=\; \left(-67\,^{+28}_{-31} \pm 7\right)^{\circ} \;, \tag{37}$$

where the first errors are statistical and the second systematic. Only a marginal constraint on δ_{+-} is obtained for C.L. < 0.05.

Finally, following the same procedure, we can also derive a constraint on α from the measured U and I coefficients. The resulting C.L. function versus α is given in the right hand plot of Fig. 6. It includes systematic uncertainties. Ignoring the mirror solution at $\alpha + 180^{\circ}$, we find

$$\alpha \;=\; \left(113\,^{+27}_{-17} \pm 6\right)^{\circ} \;, \tag{38}$$

where the systematic error is dominated by the uncertainties in the signal model. Only a marginal constraint on α is obtained for C.L. < 0.05.

7 SUMMARY

We have presented the preliminary measurement of *CP*-violating asymmetries in $B^0 \to \pi^+\pi^-\pi^0$ decays dominated by the ρ resonance. The results are obtained from a data sample of 213 millions $\Upsilon(4S) \to B\overline{B}$ decays. We extend the previous quasi-two-body approach by using a time-dependent Dalitz plot analysis. From the measurement of the coefficients of 16 form factor bilinears we determine the three *CP*-violating and two *CP*-conserving quasi-two-body parameters, where we find a 2.9σ evidence of direct *CP* violation. Taking advantage of the interference between the ρ resonances in the Dalitz plot, we derive constraints on the relative strong phase between B^0 decays to $\rho^-\pi^+$ and $\rho^+\pi^-$, and on the angle α of the Unitarity Triangle. These measurements are consistent with the expectation from the CKM fit [23].

8 ACKNOWLEDGMENTS

We are grateful for the extraordinary contributions of our PEP-II colleagues in achieving the excellent luminosity and machine conditions that have made this work possible. The success of this project also relies critically on the expertise and dedication of the computing organizations that support *BABAR*. The collaborating institutions wish to thank SLAC for its support and the kind hospitality extended to them. This work is supported by the US Department of Energy and National Science Foundation, the Natural Sciences and Engineering Research Council (Canada), Institute of High Energy Physics (China), the Commissariat à l'Energie Atomique and Institut National de Physique Nucléaire et de Physique des Particules (France), the Bundesministerium für Bildung und Forschung and Deutsche Forschungsgemeinschaft (Germany), the Istituto Nazionale di Fisica Nucleare (Italy), the Foundation for Fundamental Research on Matter (The Netherlands), the Research Council of Norway, the Ministry of Science and Technology of the Russian Federation, and the Particle Physics and Astronomy Research Council (United Kingdom). Individuals have received support from CONACyT (Mexico), the A. P. Sloan Foundation, the Research Corporation, and the Alexander von Humboldt Foundation.

References

[1] *BABAR* Collaboration (B. Aubert *et al.*), Phys. Rev. Lett. **89**, 201802 (2002).

[2] Belle Collaboration (K. Abe *et al.*), Phys. Rev. D **66**, 071102 (2002).

[3] N. Cabibbo, Phys. Rev. Lett. **10**, 531 (1963); M. Kobayashi and T. Maskawa, Prog. Theor. Phys. **49**, 652 (1973).

[4] *BABAR* Collaboration, B. Aubert *et al.*, Phys. Rev. Lett. **89**, 281802 (2002); A. Jawahery, Int. J. Mod. Phys. A **19**, 975 (2004)

[5] Belle Collaboration (K. Abe *et al.*), BELLE-PREPRINT-2004-1, hep-ex/0401029 (2004).

[6] *BABAR* Collaboration (B. Aubert *et al.*), *BABAR*-PUB-04-09, hep-ex/0404029 (2004).

[7] M. Gronau and D. London, *Phys. Rev. Lett.* **65**, 3381 (1990).

[8] H.J. Lipkin, Y. Nir, H.R. Quinn and A. Snyder, Phys. Rev. **D44**, 1454 (1991).

[9] H.R. Quinn and A.E. Snyder, Phys. Rev. **D48**, 2139 (1993).

[10] *BABAR* Collaboration (B. Aubert *et al.*), Phys. Rev. Lett. **91**, 201802 (2003); updated preliminary results at *BABAR*-PLOT-0055 (2003).

[11] ALEPH Collaboration, (R. Barate *et al.*), Z. Phys. **C76**, 15 (1997); we use updated lineshape fits including new data from e^+e^- annihilation [13] and τ spectral functions [14] (masses and widths in MeV/c^2): $m_{\rho^{\pm}(770)} = 775.5 \pm 0.6$, $m_{\rho^0(770)} = 773.1 \pm 0.5$, $\Gamma_{\rho^{\pm}(770)} = 148.2 \pm 0.8$, $\Gamma_{\rho^{\pm}(770)} = 148.0 \pm 0.9$, $m_{\rho(1450)} = 1409 \pm 12$, $\Gamma_{\rho(1450)} = 500 \pm 37$, $a_{\rho'} = 0.166 \pm 0.005$, $\phi_{\rho'} = 177.8 \pm 5.2$, $m_{\rho(1700)} = 1749 \pm 20$, $\Gamma_{\rho(1700)} \equiv 235$, $a_{\rho''} = 0.071 \pm 0.006$ and $\phi_{\rho''} \equiv 0$.

[12] The *BABAR* Physics Book, Editors P.F. Harrison and H.R. Quinn, SLAC-R-504 (1998).

[13] R.R. Akhmetshin *et al.* (CMD-2 Collaboration), *Phys. Lett.* **B527**, 161 (2002).

[14] ALEPH Collaboration, ALEPH 2002-030 CONF 2002-019, (July 2002).

[15] G.J. Gounaris and J.J. Sakurai, Phys. Rev. Lett. **21**, 244 (1968).

[16] H.R. Quinn and J. Silva, Phys. Rev. **D62**, 054002 (2000).

[17] *BABAR* Collaboration, B. Aubert *et al.*, Nucl. Instrum. Methods **A479**, 1 (2002).

[18] *BABAR* Collaboration, B. Aubert *et al.*, Phys. Rev. **D66**, 032003 (2002).

[19] Particle Data Group (S. Eidelman *et al.*), Phys. Lett. B592, 1 (2004).

[20] T. Skwarnicki, DESY F31-86-02, Ph.D. thesis (1986); see also Ref. [18].

[21] ARGUS Collaboration (H. Albrecht *et al.*), Z. Phys. C **48**, 543 (1990; see also Ref. [18]).

[22] *BABAR* Collaboration (B. Aubert *et al.*), BABAR-PUB-03-037, hep-ex/0311049 (2003)

[23] J. Charles *et al.*, hep-ph/0406184 (2004).